Direct Monitoring of Conical Intersection Passage via Electronic Coherences in Twisted X-Ray Diffraction

Haiwang Yong,[1,2,*] Jérémy R. Rouxel,[3] Daniel Keefer,[1,2] and Shaul Mukamel[1,2,†]
[1] *Department of Chemistry, University of California, Irvine, California 92697, USA*
[2] *Department of Physics and Astronomy, University of California, Irvine, California 92697, USA*
[3] *University Lyon, UJM-Saint-Étienne, CNRS, Graduate School Optics Institute, Laboratoire Hubert Curien UMR 5516, Saint-Étienne 42023, France*

(Received 22 February 2022; revised 7 April 2022; accepted 5 August 2022; published 30 August 2022)

Quantum coherences in electronic motions play a critical role in determining the pathways and outcomes of virtually all photophysical and photochemical molecular processes. However, the direct observation of electronic coherences in the vicinity of conical intersections remains a formidable challenge. We propose a novel time-resolved twisted x-ray diffraction technique that can directly monitor the electronic coherences created as the molecule passes through a conical intersection. We show that the contribution of electronic populations to this signal is canceled out when using twisted x-ray beams that carry a light orbital angular momentum, providing a direct measurement of transient electronic coherences in gas-phase molecules.

DOI: 10.1103/PhysRevLett.129.103001

The standard treatment of excited-state chemistry of molecules is based on the adiabatic separation of nuclear and electronic dynamics, known as the Born-Oppenheimer approximation. This widely used approximation breaks down when electronic and nuclear motions occur on a similar timescale and become strongly coupled. Conical intersections (CIs) are important examples where two or more adiabatic potential energy surfaces (PESs) become degenerate, resulting in strong nonadiabatic couplings between them. Because these regions allow for efficient, nonradiative electronic relaxations, they play critical roles in virtually all nonadiabatic reaction dynamics including photodissociation, isomerization, charge, and energy transfer. Notable examples include the formation of vitamin D [1], photoinduced DNA damage [2], primary events in human vision [3], and charge transfer in organic photovoltaic devices [4]. The conventional experimental signatures of CIs are indirect and based on electronic populations such as the fast conversion rates of electronic states or nuclear wave-packet bifurcation events [5–9]. The direct experimental observation of transient electronic coherences generated as the molecule passes through a CI remains a formidable task as most contemporary ultrafast measurements are dominated by the signals from electronic populations which are significantly stronger than those from electronic coherences and are not specific to CIs.

In this theoretical Letter, we propose a novel ultrafast diffraction technique that can exclusively track electronic coherences at conical intersections with no contributions from electronic populations. In contrast to previously proposed stimulated ultrafast x-ray Raman techniques that probe the energy profiles of electronic coherences [10], this technique directly images their spatial profiles through transient charge densities in the vicinity of a CI. We propose to use an optical pump laser to excite a gas-phase molecule (thiophenol) and probe its CI dynamics by ultrafast nonresonant x-ray diffraction (XRD) using twisted x-ray beams which carry orbital angular momentum (OAM). The magnitude l of the OAM is unbounded and can have any integer value. Rapid developments of both time-resolved gas-phase x-ray [11–13] and electron [8,14,15] diffraction techniques provide opportunities for tracking ultrafast structural changes, "molecular movies," during chemical reactions with atomistic spatial and femtosecond temporal resolution. Theoretical studies have shown that standard ultrafast x-ray diffraction contains a mixed elastic-inelastic coherence term originating from electronic coherences [16–19]. During the passage through a CI, the mixed coherence term is found to be significantly ($\sim$4 orders of magnitude) weaker than the dominating elastic scattering contributions that originated from electronic populations [20]. Therefore, probing electronic coherences near a CI remains experimentally challenging for conventional (plane-wave) time-resolved diffraction.

Here, we show that this major obstacle can be overcome by measuring the rotationally averaged time-resolved x-ray diffraction signals, using twisted x-ray beams carrying positive (l) and negative OAM ($-l$). It has been shown theoretically that the linear polarization of the optical pump laser could induce a partial alignment in an isotropic gas sample resulting in anisotropic x-ray scattering patterns [21–23]. This concept has been applied in ultrafast x-ray scattering experiments to distinguish initially excited electronic states [24] and multiphoton excitation channels [25]. Here, we focus on the isotropic signal that contains the complete information about the molecule in the molecular frame, which can be extracted from the overall experimental pattern using Legendre decomposition [21]. The rotationally averaged ultrafast twisted XRD is obtained by taking the difference between the l and $-l$ XRD signals: $\Delta S_l(q,T) = \langle S_l(\mathbf{q},T)\rangle_\Omega - \langle S_{-l}(\mathbf{q},T)\rangle_\Omega$, where $S_l(q,T)$ denotes the ultrafast XRD pattern recorded with a twisted beam carrying a l OAM, q is the norm of the momentum transfer vector $\mathbf{q}$, T is the time delay between the actinic pulse and the XRD process, and $\langle\ldots\rangle_\Omega$ denotes the rotationally averaged diffraction signal. We find that when taking the difference of $S_l(q,T)$ and $S_{-l}(q,T)$, the contributions of electronic populations cancel out and only the desired electronic coherences survive. The proposed technique provides a direct measurement of the passage through CIs imprinted in the transient electronic coherences. Twisted beams, also known as vortex or OAM beams, possess a wave front that twists along the beam propagation, independently of the beam polarization state. In this Letter we use a typical twisted light beam: linearly polarized Laguerre-Gaussian (LG) mode [26]. An example of the spatial and phase profiles of a LG beam ($l = 1$) in the transverse plane is shown in Supplemental Material [27], Fig. S1. The OAM gives a twist to the phase that rotates along the propagation axis thereby forming a helical spatial wave front. Various strategies have been developed to generate intense, hard-x-ray twisted beams at x-ray free-electron lasers (XFELs) [40–43], enabling ultrafast twisted XRD of free molecules. Our proposed technique depends on twisted beams in an essential way and cannot be achieved with circular polarized light only carrying spin angular moment (SAM), as the SAM of light does not engage with the molecular charge density during the scattering process making it identical to XRD of plane waves.

A molecular system driven by an optical laser can be described by the total time-dependent molecular many-body wave function which can be expanded in the adiabatic basis

$$\Psi(\mathbf{r},\mathbf{R},T) = \sum_k c_k(T)\chi_k(\mathbf{R},T)\varphi_k(\mathbf{r},\mathbf{R}), \tag{1}$$

where k labels the adiabatic electronic states, $\chi_k(\mathbf{R},T)$ is the normalized nuclear wave packet in the adiabatic electronic state $\varphi_k(\mathbf{r},\mathbf{R})$, $\mathbf{r}$ and $\mathbf{R}$ are the electronic and nuclear coordinates, and $c_k(T)$ is the electronic state amplitude. Using Eq. (1), the time-evolving molecular charge density in real space is given by

$$\begin{aligned}\langle\hat{\sigma}(\mathbf{r},T)\rangle &= \sum_k \rho_{kk}(T)\langle\chi_k|\hat{\sigma}_{kk}(\mathbf{r})|\chi_k\rangle \\ &\quad + 2\Re\left[\sum_{j>k}\rho_{jk}(T)\langle\chi_k|\hat{\sigma}_{kj}(\mathbf{r})|\chi_j\rangle\right] \\ &= \sigma_{\mathrm{pop}}(\mathbf{r},T) + \sigma_{\mathrm{coh}}(\mathbf{r},T).\end{aligned} \tag{2}$$

Here, $\hat{\sigma}(\mathbf{r})$ is the electronic charge-density operator, ρ is the density matrix operator, $\rho_{kk}(T) = c_k^*(T)c_k(T)$ are real numbers representing the electronic populations at time T while the coherence terms, $\rho_{jk}(T) = c_k^*(T)c_j(T)$ with $j \neq k$, consists of complex numbers. The electronic coherence is obtained from the combined electronic-nuclear wave function as the overlap of the nuclear wave packets. The total electronic charge density contains contributions from both time-evolving electronic population density $\sigma_{\mathrm{pop}}(\mathbf{r},T)$ and transition density $\sigma_{\mathrm{coh}}(\mathbf{r},T)$. Upon transition to an excited electronic state, the electronic coherence of the system gradually builds up as the wave packet passes the CI region where the nonadiabatic coupling is strong [44]. Probing the time evolution of this electronic coherence thus provides direct evidence for the presence of the CI and offers a convenient way for monitoring CI dynamics.

The theoretical description of the time-resolved twisted XRD signal is based on the off-resonant single-molecule (gas-phase) time-resolved XRD in the minimal coupling picture [17,45]. Similar to Eq. (2), the time-resolved twisted XRD signal can be partitioned into the sum of contributions from electronic populations $S_l^{\mathrm{pop}}(\mathbf{q},T)$ and coherences $S_l^{\mathrm{coh}}(\mathbf{q},T)$ (see details in Supplemental Material [27], Note 1),

$$S_l(\mathbf{q},T) = S_l^{\mathrm{pop}}(\mathbf{q},T) + S_l^{\mathrm{coh}}(\mathbf{q},T). \tag{3}$$

It is well known that the scattering of plane-wave photons results in centrosymmetric diffraction patterns, $S_0(\mathbf{q}) = S_0(-\mathbf{q})$, as stated by Friedel's law, which, however, does not hold for twisted beams [46]. As illustrated in Supplemental Material [27], Fig. S1, diffraction patterns of x-ray beams carrying OAM ($l = \pm 1$ patterns) for an oriented molecule are no longer centrosymmetric, unlike the standard x-ray ($l = 0$) diffraction pattern. In addition, it has been demonstrated for static objects like apertures or crystals that x-ray diffraction patterns of twisted beams with opposite OAM (l) are linked by an inversion operation $S_l(\mathbf{q}) = S_{-l}(-\mathbf{q})$ [46]. Turning to time-resolved diffraction from molecules, we find that this inversion relation still holds for the population contribution S_l^{pop}, i.e., $S_l^{\mathrm{pop}}(\mathbf{q},T) = S_{-l}^{\mathrm{pop}}(-\mathbf{q},T)$, but not for the coherence contribution $S_l^{\mathrm{coh}}(\mathbf{q},T)$ due to its mixed elastic-inelastic character and the presence of the complex electronic coherence terms ρ_{jk} (see Supplemental Material [27], Note 1). A ground-state molecule only has a population contribution thus its $l = 1$ pattern is rotated by π rad with respect to the $l = -1$ as shown in Supplemental Material [27], Fig. S1.

We next investigate the rotationally averaged difference signal of gas-phase molecules

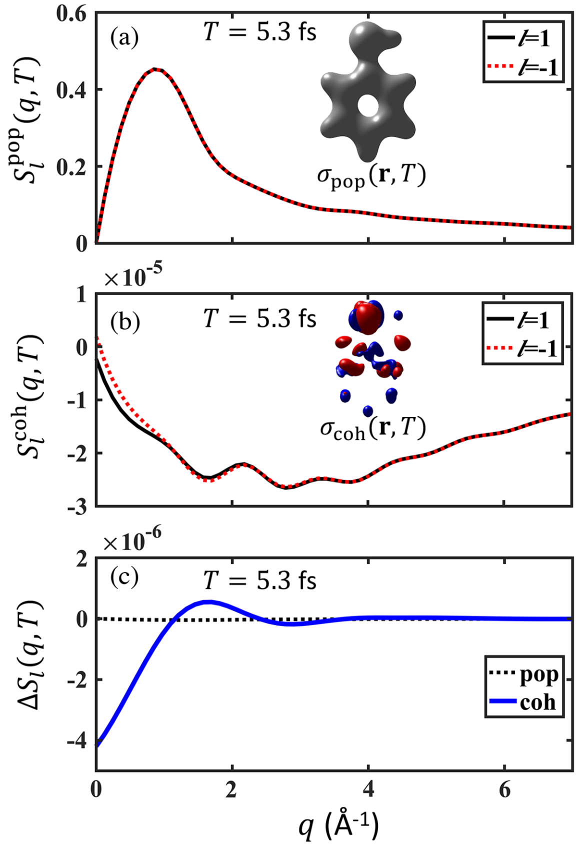

FIG. 1. Rotationally averaged diffraction signal at $T = 5.3$ fs after excitation. Population contribution $S_{l=\pm1}^{\rm pop}$ (top), coherence contribution $S_{l=\pm1}^{\rm coh}$ (middle) and difference signal $\Delta S_{l=1}^{\rm pop/coh} = S_{l=1}^{\rm pop/coh} - S_{l=-1}^{\rm pop/coh}$ (bottom). Insets: Isosurface plots of time-evolving population $\sigma_{\rm pop}$ (top) and coherent $\sigma_{\rm coh}$ (middle) charge densities in real space at $T = 5.3$ fs.

$$\begin{aligned}\Delta S_l(q,T) &= \langle S_l(\mathbf{q},T)\rangle_\Omega - \langle S_{-l}(\mathbf{q},T)\rangle_\Omega \\ &= \Delta S_l^{\rm pop}(q,T) + \Delta S_l^{\rm coh}(q,T). \qquad (4)\end{aligned}$$

One can immediately see that $\Delta S_l^{\rm pop}(q,T) = \langle S_l^{\rm pop}(\boldsymbol{q},T)\rangle_\Omega - \langle S_{-l}^{\rm pop}(\boldsymbol{q},T)\rangle_\Omega = 0$ from the centrosymmetric relation $S_l^{\rm pop}(\mathbf{q},T) = S_{-l}^{\rm pop}(-\mathbf{q},T)$, which implies a vanishing population contribution $\Delta S_l^{\rm pop}(q,T) = 0$. Because the coherence term is not centrosymmetric $[S_l^{\rm coh}(\mathbf{q},T) \neq S_{-l}^{\rm coh}(-\mathbf{q},T)]$, we obtain a purely electronic coherence signal $\Delta S_l(q,T) = \Delta S_l^{\rm coh}(q,T)$ with no contributions from electronic population. $\Delta S_l(q,T)$ is constructed by elements of the electronic coherence terms and the momentum-space electronic charge-density operators which carry OAM, $\hat{\sigma}_l(\mathbf{q}) = \int \hat{\sigma}(\mathbf{r}) e^{il\phi} e^{i\mathbf{q}\cdot\mathbf{r}} d\mathbf{r}$. The signal amplitude of $\Delta S_l(q,T)$ is no longer derived from the simple Fourier transform of $\hat{\sigma}(\mathbf{r})$ as in standard XRD, but contains the phase twist ($e^{il\phi}$) which is the source of the coherence discrimination. $\Delta S_l(q,T)$ is derived in Supplemental Material [27], Note 2.

We demonstrate the power of the proposed technique by applying it to a realistic and accessible molecular system (thiophenol photodissociation involving two CIs) calculated by exact quantum dynamical simulations. The corresponding Hamiltonian based on fully *ab initio* quantum chemical simulations was introduced previously [47]. Two CIs, S_2/S_1 and S_1/S_0, were identified along the S-H dissociation channels in the course of the nonadiabatic relaxation process [48,49]. In addition to S-H stretching, the in-plane S-H bending mode is known to be active in the conical intersection dynamics [50]. Quantum dynamical simulations were performed by numerically solving the time-dependent Schrödinger equation for nuclei on the adiabatic potential energy surfaces of these two reactive coordinates (S-H distance and H-S-C angle), allowing for a fully quantum mechanical treatment of both electrons and nuclei, and including nonadiabatic couplings at the conical intersections. Since only two nuclear degrees of freedom contribute to the branching space of a conical intersection while the energy along all other degrees of freedom remains degenerate, quantum dynamical simulations of two reactive coordinates are commonly used to describe nonadiabatic dynamics in conical intersections [51–55]. We note that the signal would be scaled down proportionally to the reduced degree of coherence if a full dimensional rather than reduced dimensionality model is used. For the ultrafast thiophenol S-H dissociation, the nuclear wave packet is coherently funneled into small reactive degrees of freedom, which exhibit by far the largest energy gradients that are captured in our Hamiltonian, as there is no time for many nuclear space degrees of freedom to be explored in sub-40 fs timescale considered in this Letter. The simulated nuclear wave packet dynamics has been discussed in detail elsewhere [47]. The resulting dynamical pathways are sketched in Supplemental Material [27], Fig. S1. Briefly, upon excitation to S_2, the wave packet first reaches the S_2/S_1 CI within 10 fs and then bifurcates into two pathways. One portion of the nuclear wave packet travels to the Franck-Condon region and localized on the S_1 surface, while the other part continues to pass the S_1/S_0 CI leading to hydrogen dissociation within 40 fs. We note that for much longer timescales (>40 fs) our Hamiltonian may not be valid since it misses internal vibrational relaxation to other nuclear degrees of freedom and dissipation effects. A two-dimensional model Hamiltonian could then overestimate the magnitude of electronic coherence.

We have used the total molecular wave function of thiophenol to simulate the time-resolved rotationally averaged diffraction signals, $S_l(q,T)$ for $l = 1$ and $l = -1$ OAM x-ray beams. Figures 1(a) and 1(b) show the simulated results for both population contributions, $S_{l=\pm1}^{\rm pop}$, and coherence contributions, $S_{l=\pm1}^{\rm coh}$ at 5.3 fs time delay. It is clear that the population contribution to the time-resolved signal is identical for $l = 1$ and $l = -1$ OAM light, while their coherence contributions are distinct.

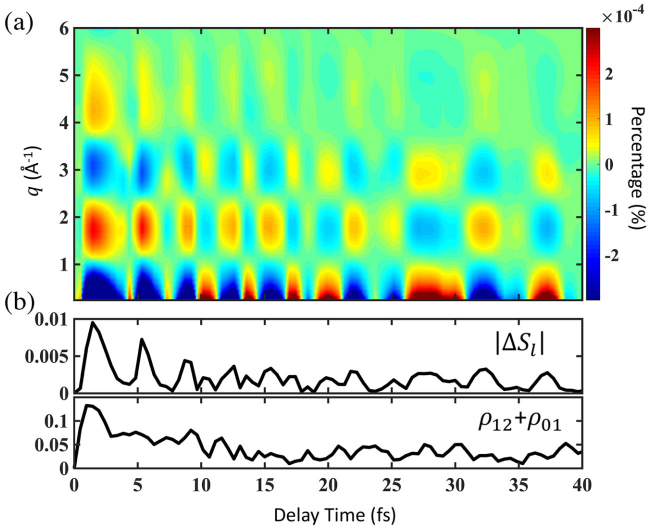

FIG. 2. (a) Rotationally averaged time-resolved difference signals, $\Delta S_{l=1}(q, T)$, in Eq. (4). The signals are shown as percentages, $100[\Delta S_{l=1}(q, T)/S^{\mathrm{off}}_{l=1}(q)]$, where $S^{\mathrm{off}}_{l=1}(q)$ is the reference x-ray diffraction signal before time zero. (b) Absolute value of the difference signal in (a) integrated over q (top) and the total coherence magnitude of the $\mathrm{S}_2/\mathrm{S}_1$ and $\mathrm{S}_1/\mathrm{S}_0$ electronic coherences calculated by quantum dynamics (bottom).

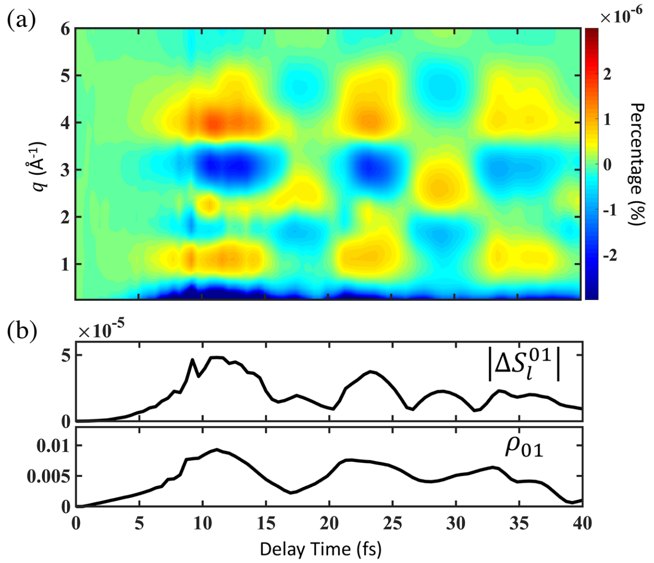

FIG. 3. Same as Fig. 2 but only for the $\mathrm{S}_1/\mathrm{S}_0$ electronic coherence.

Figure 1(c) demonstrates that the population contribution to the isotropic difference signal $\Delta S^{\mathrm{pop}}_{l}(q, T)$ vanishes so that $\Delta S_l(q, T) = \Delta S^{\mathrm{coh}}_{l}(q, T)$. We note that both population and coherence contributions appear mainly at small q values, because the time-evolving population and coherent charge densities are both diffuse and spread across the entire molecule in real space as illustrated in Fig. 1 insets. The diffraction signals at small q values could be accessed by setting the main x-ray beam off center from the hole of the detector similar to a recent ultrafast gas-phase electron diffraction setup [56].

Figure 2 depicts the total time-resolved difference signal, which originates from the time-evolving coherent charge density, σ_{coh} in Eq. (2). The time dependence of the total signal comes from the time-evolving electronic coherence terms, and its variation with q reflects the real-space distribution of the coherent charge density, revealing both temporal and spatial profiles. Since electronic coherences are only generated when the nuclear wave packet passes through the $\mathrm{S}_2/\mathrm{S}_1$ and $\mathrm{S}_1/\mathrm{S}_0$ CI, the overall signal in Fig. 2(a) results from electronic coherences at both CIs. To investigate the temporal variations of the signal in Fig. 2(a), we show the time-dependent absolute difference signal integrated over q in the top panel of Fig. 2(b). For comparison, the sum of the $\mathrm{S}_2/\mathrm{S}_1$ and $\mathrm{S}_1/\mathrm{S}_0$ electronic coherence magnitudes obtained directly from the quantum dynamical simulations is shown in the bottom panel of Fig. 2(b). The integrated difference signal closely resembles the time-dependent electronic coherences in the molecule. The sharp rise of the signal after time zero indicates that the system starts to pass the first $\mathrm{S}_2/\mathrm{S}_1$ CI shortly after the laser excitation. The signal decreases within 10 fs, indicating that the wave packet has reached the $\mathrm{S}_2/\mathrm{S}_1$ CI. The subsequent weak but finite signal up to 40 fs receives contributions from two electronic coherences: the $\mathrm{S}_2/\mathrm{S}_1$ electronic coherence generated near the Frank-Condon region when one portion of the wave packet is localized in S_1 after bifurcation, and the $\mathrm{S}_1/\mathrm{S}_0$ electronic coherence generated when the other portion of the wave packet passes the $\mathrm{S}_1/\mathrm{S}_0$ CI.

To further trace the origins of the signal in Fig. 2, we have separated out the signal contributed by the $\mathrm{S}_1/\mathrm{S}_0$ electronic coherence. Figure 3(a) clearly shows different features compared to Fig. 2(a) with different oscillation periods, demonstrating the electronic coherences generated at different CIs. We find that the signal in Fig. 3 is about 2 orders of magnitude smaller than the total signal shown in Fig. 2. This is because the $\mathrm{S}_1/\mathrm{S}_0$ electronic coherence is much weaker than $\mathrm{S}_2/\mathrm{S}_1$ ($|\rho_{01}| \ll |\rho_{12}|$) as shown in Figs. 2(b) and 3(b), as discussed in Ref. [19]. The $\mathrm{S}_1/\mathrm{S}_0$ electronic coherence is barely observable in the total signal. This is an intrinsic property of the specific system, rather than of the proposed setup. To make it detectable, one could use a different pumping strategy such as an infrared field resonant with the electronic transition in the $\mathrm{S}_1/\mathrm{S}_0$ CI region to noninvasively amplify the $\mathrm{S}_1/\mathrm{S}_0$ coherence [57]. Similar to Fig. 2(b), the difference signal integrated over q shown in Fig. 3(b) nicely monitors the time dependence of the electronic coherence ρ_{01}. The proposed setup could thus provide a direct measurement of the distinct electronic coherences generated at different CIs, potentially allowing for their experimental separation. This would open a novel window into competing quantum pathways during ultrafast reactive molecular processes.

The twisted beams required for the proposed experiment are readily available at FELs and can be implemented in an ultrafast XRD experiment by adding an optical element in the incoming x-ray beam path, e.g., spiral phase plates [43,58], or by tuning the undulator [41,42]. This setup can handle the high brilliance of XFELs pulses and can be characterized using ptychographic measurements. The ultrafast XRD setup adds the usual requirement of accurate arrival time measurements and shot-to-shot corrections. Time and pulse energy jitter diagnostics are routinely available at XFELs facilities to tackle such challenges. These diagnostics could also be valuable for correcting possible artifacts occurring when switching between positive and negative OAM twisted beams. Existing ultrafast gas-phase XRD setup [59] at LCLS (120 pulses per second) has achieved an exceptionally high signal-to-noise ratio and sensitivity to very small changes ($\sim 0.1\%$) in the percentage diffraction signal. Since the desired electronic coherence signal in this Letter requires about 3 orders of magnitude higher signal-to-noise ratio for resolving the percentage signal of $\sim 0.0001\%$ in Fig. 2, the ongoing development of high-repetition-rate hard x ray at LCLS-II (1×10^6 pulses per second) is important for the realization of the proposed experiment as it could greatly reduce dominate shot noises of ultrafast XRD experiments in gas phase [60].

We note that in our quantum dynamical simulation the initial wave packet is obtained by impulsive excitation of the ground state vibrational wave function from S_0 to S_2 (100% excitation). This leads to an overestimate of the resulting signal for a weak excitation experiment. To maximize the desired coherence signal, optimal control theory [61,62] could be employed to optimize pump pulses for efficient population transfer upon photoexcitation. In this Letter, because the nuclear wave packet rapidly travels away from the Franck-Condon region after photoexcitation due to fast S-H dissociation, the initial coherence between S_2 and S_0 in the Franck-Condon region is ignored in the simulation. However, this initial coherence could persist and contribute to the coherence signals in other dynamical processes which is worth further investigations. In addition, the effect of the energy detection window of the scattering detector has been found to play an important role in the detected scattering signal [63–65]. Here, we assume an intermediate detection window where the rovibrational transition energies of the molecule are not resolved [64]. Further extension of the effect of the detection window to twisted x-ray diffraction could provide valuable insights.

In summary, we have demonstrated a novel technique for the direct monitoring of transient electronic coherences along the passage through CIs. Diffraction signals of gas-phase molecules are measured using twisted x-ray beams carrying OAM. We have used x-ray beams with $l = \pm 1$ OAM to demonstrate that the rotationally averaged difference signal can directly monitor the time evolution of electronic coherences in a photoexcited molecule. The concept is also applicable to twisted x-ray beams with other nonzero numbers of l. The momentum profile of measurements with multiple ls could provide opportunities for reconstructing the complete time-evolving coherent charge density σ_{coh} in real space, where the concrete details and generality are subject to future studies. The direct imaging of electronic coherences in molecules opens brand new avenues for monitoring photophysical and photochemical processes, providing further opportunities for electronic coherent control over conical-intersection dynamics [66]. Since the proposed technique is sensitive to the electronic coherences but not populations, it paves the way for the direct imaging of many other fundamental coherence phenomena in molecules; for example, tracking attosecond coherent electron motions in real space and time with state of the art attosecond XFELs [67,68].

The work was primarily supported by the Chemical Sciences, Geosciences, and Biosciences Division, Office of Basic Energy Sciences, Office of Science, U.S. Department of Energy through Award No. DE-FG02-04ER15571. S. M. received support though a fellowship from the Hagler Institute for Advanced Study at Texas A&M University. Support of the National Science Foundation through Grant No. CHE-1953045 is gratefully acknowledged. J. R. R. was supported by the LABEX MANUTECH-SISE (ANR-10-LABX-0075) of Université de Lyon, within the program “Investissements d’Avenir” (ANR-11-IDEX-0007) operated by the French National Research Agency (ANR). D. K. gratefully acknowledges support from the Alexander von Humboldt foundation through the Feodor Lynen program.

The authors declare that they have no competing interests.

---

[*] Corresponding author.
h.yong@uci.edu
[†] Corresponding author.
smukamel@uci.edu

[1] E. Tapavicza, A. M. Meyer, and F. Furche, Unravelling the details of vitamin D photosynthesis by non-adiabatic molecular dynamics simulations, Phys. Chem. Chem. Phys. **13**, 20986 (2011).

[2] C. E. Crespo-Hernández, B. Cohen, P. M. Hare, and B. Kohler, Ultrafast excited-state dynamics in nucleic acids, Chem. Rev. **104**, 1977 (2004).

[3] D. Polli, P. Altoè, O. Weingart, K. M. Spillane, C. Manzoni, D. Brida, G. Tomasello, G. Orlandi, P. Kukura, R. A. Mathies, M. Garavelli, and G. Cerullo, Conical intersection dynamics of the primary photoisomerization event in vision, Nature (London) **467**, 440 (2010).

[4] S. M. Falke, C. A. Rozzi, D. Brida, M. Maiuri, M. Amato, E. Sommer, A. D. Sio, A. Rubio, G. Cerullo, E. Molinari, and C. Lienau, Coherent ultrafast charge transfer in an organic photovoltaic blend, Science **344**, 1001 (2014).

[5] A. Stolow, A. E. Bragg, and D. M. Neumark, Femtosecond time-resolved photoelectron spectroscopy, Chem. Rev. **104**, 1719 (2004).

[6] H. J. Wörner, J. B. Bertrand, B. Fabre, J. Higuet, H. Ruf, A. Dubrouil, S. Patchkovskii, M. Spanner, Y. Mairesse, V. Blanchet, E. Mével, E. Constant, P. B. Corkum, and D. M. Villeneuve, Conical intersection dynamics in NO_2 probed by homodyne high-harmonic spectroscopy, Science **334**, 208 (2011).

[7] K. S. Zinchenko, F. Ardana-Lamas, I. Seidu, S. P. Neville, J. van der Veen, V. U. Lanfaloni, M. S. Schuurman, and H. J. Wörner, Sub-7-femtosecond conical-intersection dynamics probed at the carbon K-edge, Science **371**, 489 (2021).

[8] J. Yang *et al.*, Imaging CF_3I conical intersection and photodissociation dynamics with ultrafast electron diffraction, Science **361**, 64 (2018).

[9] A. Hosselnlzadeh, N. Breckwoldt, R. Fung, R. Sepehr, M. Schmidt, P. Schwander, R. Santra, and A. Ourmazd, Few-fs resolution of a photoactive protein traversing a conical intersection, Nature (London) **599**, 697 (2021).

[10] M. Kowalewski, K. Bennett, K. E. Dorfman, and S. Mukamel, Catching Conical Intersections in the Act: Monitoring Transient Electronic Coherences by Attosecond Stimulated X-Ray Raman Signals, Phys. Rev. Lett. **115**, 193003 (2015).

[11] M. P. Minitti, J. M. Budarz, A. Kirrander, J. S. Robinson, D. Ratner, T. J. Lane, D. Zhu, J. M. Glownia, M. Kozina, H. T. Lemke, M. Sikorski, Y. Feng, S. Nelson, K. Saita, B. Stankus, T. Northey, J. B. Hastings, and P. M. Weber, Imaging Molecular Motion: Femtosecond X-Ray Scattering of an Electrocyclic Chemical Reaction, Phys. Rev. Lett. **114**, 255501 (2015).

[12] P. H. Bucksbaum, M. R. Ware, A. Natan, J. P. Cryan, and J. M. Glownia, Characterizing Multiphoton Excitation Using Time-Resolved X-Ray Scattering, Phys. Rev. X **10**, 011065 (2020).

[13] H. Yong, N. Zotev, J. M. Ruddock, B. Stankus, M. Simmermacher, A. Moreno Carrascosa, W. Du, N. Goff, Y. Chang, D. Bellshaw, M. Liang, S. Carbajo, J. E. Koglin, J. S. Robinson, S. Boutet, M. P. Minitti, A. Kirrander, and P. M. Weber, Observation of the molecular response to light upon photoexcitation, Nat. Commun. **11**, 2157 (2020).

[14] A. A. Ischenko, P. M. Weber, and R. J. Dwayne Miller, Capturing chemistry in action with electrons: Realization of atomically resolved reaction dynamics, Chem. Rev. **117**, 11066 (2017).

[15] M. Centurion, T. J. A. Wolf, and J. Yang, Ultrafast imaging of molecules with electron diffraction, Annu. Rev. Phys. Chem. **73**, 2.1 (2022).

[16] J. Cao and K. R. Wilson, Ultrafast x-ray diffraction theory, J. Phys. Chem. A **102**, 9523 (1998).

[17] U. Lorenz, K. B. Møller, and N. E. Henriksen, Theory of time-resolved inelastic x-ray diffraction, Phys. Rev. A **81**, 023422 (2010).

[18] K. Bennett, M. Kowalewski, J. R. Rouxel, and S. Mukamel, Monitoring molecular nonadiabatic dynamics with femtosecond x-ray diffraction, Proc. Natl. Acad. Sci. U.S.A. **115**, 6538 (2018).

[19] M. Simmermacher, N. E. Henriksen, K. B. Møller, A. Moreno Carrascosa, and A. Kirrander, Electronic Coherence in Ultrafast X-Ray Scattering from Molecular Wave Packets, Phys. Rev. Lett. **122**, 073003 (2019).

[20] D. Keefer, F. Aleotti, J. R. Rouxel, F. Segatta, B. Gu, A. Nenov, M. Garavelli, and S. Mukamel, Imaging conical intersection dynamics during azobenzene photoisomerization by ultrafast x-ray diffraction, Proc. Natl. Acad. Sci. U.S.A. **118**, e2022037118 (2021).

[21] U. Lorenz, K. B. Møller, and N. E. Henriksen, On the interpretation of time-resolved anisotropic diffraction patterns, New J. Phys. **12**, 113022 (2010).

[22] K. B. Møller and N. E. Henriksen, Time-resolved x-ray diffraction: The dynamics of the chemical bond, in *Molecular Electronic Structures of Transition Metal Complexes I: Structure and Bonding,* edited by D. Mingos, P. Day, and J. Dahl (Springer, Berlin, Heidelberg, 2012), Vol. 142, pp. 185–211.

[23] M. Simmermacher, A. Kirrander, and N. E. Henriksen, Time-resolved x-ray scattering from impulsively aligned or oriented molecules, Phys. Rev. A **102**, 052825 (2020).

[24] H. Yong, N. Zotev, B. Stankus, J. M. Ruddock, D. Bellshaw, S. Boutet, T. J. Lane, M. Liang, S. Carbajo, J. S. Robinson, W. Du, N. Goff, Y. Chang, J. E. Koglin, M. D. J. Waters, T. I. Sølling, M. P. Minitti, A. Kirrander, and P. M. Weber, Determining orientations of optical transition dipole moments using ultrafast x-ray scattering, J. Phys. Chem. Lett. **9**, 6556 (2018).

[25] A. Natan, A. Schori, G. Owolabi, J. P. Cryan, J. M. Glownia, and P. H. Bucksbaum, Resolving multiphoton processes with high-order anisotropy ultrafast x-ray scattering, Faraday Discuss. **228**, 123 (2021).

[26] L. Allen, M. W. Beijersbergen, R. J. C. Spreeuw, and J. P. Woerdman, Orbital angular momentum of light and the transformation of Laguerre-Gaussian laser modes, Phys. Rev. A **45**, 8185 (1992).

[27] See Supplemental Material at http://link.aps.org/supplemental/10.1103/PhysRevLett.129.103001 for notes on (1) twisted x-ray diffraction signal, (2) the purely electronic coherence signal, (3) wave packet simulations, and (4) computational details, which includes Fig. S1 and Refs. [28–39].

[28] P. H. Berens and K. R. Wilson, Molecular dynamics and spectra. I. Diatomic rotation and vibration, J. Chem. Phys. **74**, 4872 (1981).

[29] S. Thallmair, M. K. Roos, and R. de Vivie-Riedle, Design of specially adapted reactive coordinates to economically compute potential and kinetic energy operators including geometry relaxation, J. Chem. Phys. **144**, 234104 (2016).

[30] H. Tal-Ezer and R. Kosloff, An accurate and efficient scheme for propagating the time dependent Schrödinger equation, J. Chem. Phys. **81**, 3967 (1984).

[31] S. Butterworth, On the theory of filter amplifiers, Exp. Wireless Wireless Eng. **7**, 536 (1930).

[32] H.-J. Werner, P. J. Knowles, F. R. Manby, J. A. Black, K. Doll, A. Heßelmann, D. Kats, A. Köhn, T. Korona, D. A. Kreplin *et al.*, The Molpro quantum chemistry package, J. Chem. Phys. **152**, 144107 (2020).

[33] H. J. Werner, P. J. Knowles, G. Knizia, F. R. Manby, and M. Schütz, Molpro: A general-purpose quantum chemistry program package, Wiley Interdiscip. Rev. Comput. Mol. Sci. **2**, 242 (2012).

[34] Q. Sun, T. C. Berkelbach, N. S. Blunt, G. H. Booth, S. Guo, Z. Li, J. Liu, J. McClain, S. Sharma, S. Wouters *et al.*, PySCF: The Python-based simulations of chemistry framework, Comput. Mol. Sci. **8**, e1340 (2018).

[35] Q. Sun, X. Zhang, S. Banerjee, P. Bao, M. Barbry, N. S. Blunt, N. A. Bogdanov, G. H. Booth, J. Chen, Z.-H. Cui *et al.*, Recent developments in the PySCF program package, J. Chem. Phys. **153**, 024109 (2020).

[36] R. M. Parrish and T. J. Martínez, *Ab initio* computation of rotationally-averaged pump-probe x-ray and electron diffraction signals, J. Chem. Theory Comput. **15**, 1523 (2019).

[37] T. Northey, N. Zotev, and A. Kirrander, Ab initio calculation of molecular diffraction, J. Chem. Theory Comput. **10**, 4911 (2014).

[38] A. Moreno Carrascosa, H. Yong, D. L. Crittenden, P. M. Weber, and A. Kirrander, *Ab initio* calculation of total x-ray scattering from molecules, J. Chem. Theory Comput. **15**, 2836 (2019).

[39] N. Zotev, A. Moreno Carrascosa, M. Simmermacher, and A. Kirrander, Excited electronic states in total isotropic scattering from molecules, J. Chem. Theory Comput. **16**, 2594 (2020).

[40] E. Hemsing, A. Marinelli, and J. B. Rosenzweig, Generating Optical Orbital Angular Momentum in a High-Gain Free-Electron Laser at the First Harmonic, Phys. Rev. Lett. **106**, 164803 (2011).

[41] E. Hemsing, A. Knyazik, M. Dunning, D. Xiang, A. Marinelli, C. Hast, and J. B. Rosenzweig, Coherent optical vortices from relativistic electron beams, Nat. Phys. **9**, 549 (2013).

[42] J. Bahrdt, K. Holldack, P. Kuske, R. Müller, M. Scheer, and P. Schmid, First Observation of Photons Carrying Orbital Angular Momentum in Undulator Radiation, Phys. Rev. Lett. **111**, 034801 (2013).

[43] F. Seiboth, M. Kahnt, M. Lyubomirskiy, M. Seyrich, F. Wittwer, T. Ullsperger, S. Nolte, D. Batey, C. Rau, and C. G. Schroer, Refractive hard x-ray vortex phase plates, Opt. Lett. **44**, 4622 (2019).

[44] G. D. Scholes, G. R. Fleming, L. X. Chen, A. Aspuru-Guzik, A. Buchleitner, D. F. Coker, G. S. Engel, R. van Grondelle, A. Ishizaki, D. M. Jonas, J. S. Lundeen, J. K. McCusker, S. Mukamel, J. P. Ogilvie, A. Olaya-Castro, M. A. Ratner, F. C. Spano, K. B. Whaley, and X. Zhu, Using coherence to enhance function in chemical and biophysical systems, Nature (London) **543**, 647 (2017).

[45] J. R. Rouxel, M. Kowalewski, K. Bennett, and S. Mukamel, X-Ray Sum Frequency Diffraction for Direct Imaging of Ultrafast Electron Dynamics, Phys. Rev. Lett. **120**, 243902 (2018).

[46] R. Juchtmans, G. Guzzinati, and J. Verbeeck, Extension of Friedel's law to vortex-beam diffraction, Phys. Rev. A **94**, 033858 (2016).

[47] H. Yong, D. Keefer, and S. Mukamel, Imaging purely nuclear quantum dynamics in molecules by combined x-ray and electron diffraction, J. Am. Chem. Soc. **144**, 7796 (2022).

[48] I. S. Lim, J. S. Lim, Y. S. Lee, and S. K. Kim, Experimental and theoretical study of the photodissociation reaction of thiophenol at 243 nm: Intramolecular orbital alignment of the phenylthiyl radical, J. Chem. Phys. **126**, 034306 (2007).

[49] M. N. R. Ashfold, A. L. Devine, R. N. Dixon, G. A. King, M. G. D. Nix, and T. A. A. Oliver, Exploring nuclear motion through conical intersections in the UV photodissociation of phenols and thiophenol, Proc. Natl. Acad. Sci. U.S.A. **105**, 12701 (2008).

[50] H. S. You, S. Han, J. S. Lim, and S. K. Lim, $(\pi\pi^*/\pi\sigma^*)$ conical intersection seam experimentally observed in the S-D bond dissociation reaction of thiophenol-D1, J. Phys. Chem. Lett. **6**, 3202 (2015).

[51] C. Woywod, W. Domcke, A. L. Sobolewski, and H.-J. Werner, Characterization of the $S_1 - S_2$ conical intersection in pyrazine using ab initio multiconfiguration self-consistent-field and multireference configuration-interaction methods, J. Chem. Phys. **100**, 1400 (1994).

[52] S. Hahn and G. Stock, Quantum-mechanical modeling of the femtosecond isomerization in rhodopsin, J. Phys. Chem. B **104**, 1146 (2000).

[53] A. Hofmann and R. de Vivie-Riedle, Quantum dynamics of photoexcited cyclohexadiene introducing reactive coordinates, J. Chem. Phys. **112**, 5054 (2000).

[54] H.-G. Duan and M. Thorwart, Quantum mechanical wave packet dynamics at a conical intersection with strong vibrational dissipation, J. Phys. Chem. Lett. **7**, 382 (2016).

[55] D. Dey and N. E. Henriksen, On weak-field (one-photon) coherent control of photoisomerization, J. Phys. Chem. Lett. **11**, 8470 (2020).

[56] J. Yang, X. Zhu, J. P. F. Nunes, J. K. Yu, R. M. Parrish, T. J. A. Wolf, M. Centurion, M. Gühr, R. Li, Y. Liu, B. Moore, M. Niebuhr, S. Park, X. Shen, S. Weathersby, T. Weinacht, T. J. Martinez, and X. Wang, Simultaneous observation of nuclear and electronic dynamics by ultrafast electron diffraction, Science **368**, 885 (2020).

[57] D. Keefer, J. R. Rouxel, F. Aleotti, F. Segatta, M. Garavelli, and S. Mukamel, Diffractive imaging of conical intersections amplified by resonant infrared fields, J. Am. Chem. Soc. **143**, 13806 (2021).

[58] P. R. Ribič, B. Rösner, D. Gauthier, E. Allaria, F. Döring, L. Foglia, L. Giannessi, N. Mahne, M. Manfredda, C. Masciovecchio, R. Mincigrucci, N. Mirian, E. Principi, E. Roussel, A. Simoncig, S. Spampinati, C. David, and G. De Ninno, Extreme-Ultraviolet Vortices from a Free-Electron Laser, Phys. Rev. X **7**, 031036 (2017).

[59] B. Stankus, H. Yong, J. Ruddock, L. Ma, A. M. Carrascosa, N. Goff, S. Boutet, X. Xu, N. Zotev, A. Kirrander, M. P. Minitti, and P. M. Weber, Advances in ultrafast gas-phase x-ray scattering, J. Phys. B **53**, 234004 (2020).

[60] L. Ma, H. Yong, J. D. Geiser, A. Moreno Carrascosa, N. Goff, and P. M. Weber, Ultrafast x-ray and electron scattering of free molecules: A comparative evaluation, Struct. Dyn. **7**, 034102 (2020).

[61] R. S. Judson and H. Rabitz, Teaching Lasers to Control Molecules, Phys. Rev. Lett. **68**, 1500 (1992).

[62] H. Rabitz, R. de Vivie-Riedle, M. Motzkus, and K. Kompa, Whither the future of controlling quantum phenomena?, Science **288**, 824 (2000).

[63] G. Dixit, J. M. Slowik, and R. Santra, Theory of time-resolved nonresonant x-ray scattering for imaging ultrafast coherent electron motion, Phys. Rev. A **89**, 043409 (2014).

[64] M. Simmermacher, A. Moreno Carrascosa, N. E. Henriksen, K. B. Møller, and A. Kirrander, Theory of ultrafast x-ray

scattering by molecules in the gas phase, J. Chem. Phys. **151**, 174302 (2019).

[65] J. R. Rouxel, D. Keefer, and S. Mukamel, Signatures of electronic and nuclear coherences in ultrafast molecular x-ray and electron diffraction, Struct. Dyn. **8**, 014101 (2021).

[66] M. F. Kling, P. von den Hoff, I. Znakovskaya, and R. de Vivie-Riedle, (Sub-)femtosecond control of molecular reactions via tailoring the electric field of light, Phys. Chem. Chem. Phys. **15**, 9448 (2013).

[67] S. Huang, Y. Ding, Y. Feng, E. Hemsing, Z. Huang, J. Krzywinski, A. A. Lutman, A. Marinelli, T. J. Maxwell, and D. Zhu, Generating Single-Spike Hard X-Ray Pulses with Nonlinear Bunch Compression in Free-Electron Lasers, Phys. Rev. Lett. **119**, 154801 (2017).

[68] J. Duris *et al.*, Tunable isolated attosecond x-ray pulses with gigawatt peak power from a free-electron laser, Nat. Photonics **14**, 30 (2020).

Supplementary Material for

Direct Monitoring of Conical Intersection Passage via Electronic Coherences in Twisted X-Ray Diffraction

Haiwang Yong*, Jérémy R. Rouxel, Daniel Keefer, Shaul Mukamel*

*Correspondence to: smukamel@uci.edu (S. M.); h.yong@uci.edu (H. Y.)

Note 1. Twisted X-ray Diffraction Signal

The off-resonant single-molecule (gas-phase) X-ray diffraction signal in the minimal coupling picture is given by (*1,2*)

$$S(\mathbf{q},T) \propto \int d\mathbf{r}d\mathbf{r}'dt\, \mathcal{A}_X(\mathbf{r},t-T)\mathcal{A}_X^*(\mathbf{r}',t-T)\langle\hat{\sigma}^\dagger(\mathbf{r}',t)\hat{\sigma}(\mathbf{r},t)\rangle e^{i\mathbf{q}\cdot(\mathbf{r}-\mathbf{r}')} \tag{S1}$$

where $\mathcal{A}_X$ is the probe vector potential, $\hat{\sigma}(\mathbf{r},t)$ is the charge-density operators. In Eq. 1, we assume an ultrashort probe pulse so that $t = t'$. The vector potential $\mathcal{A}_X$ of twisted light beams is given by

$$\mathcal{A}_X(\mathbf{r},t) = E(t)\mathcal{A}_l(r,z,\phi) = E(t)A(r,z)e^{il\phi} \tag{S2}$$

where $A(r,z)$ is the radial profile of the beam at height z and $E(t)$ is the temporal profile. The angular index l is called the topological charge of the twisted beam. Twisted beams are eigenstates of the angular momentum operator, and possess an orbital angular momentum (OAM) of $l\hbar$ per photon. Here we express the beam profile in cylindrical coordinates, where r is the radial distance, ϕ is angular coordinate and z is axial coordinate. In this study we use a typical twisted Laguerre-Gaussian (LG) beam (*3*). LG beams are determined by angular index l and radial index p, and their spatial profile is given by

$$\mathrm{LG}_{lp}(r,z,\phi) = \frac{\sqrt{\frac{2p!}{\pi(p+|l|)!}}}{w(z)}\left(\frac{\sqrt{2}r}{w(z)}\right)^{|l|} e^{-\frac{r^2}{w^2(z)}-ik\frac{r^2}{2R(z)}} L_p^{|l|}\left(\frac{2r^2}{w^2(z)}\right) e^{i(2p+|l|+1)\tan^{-1}(\frac{z}{z_R})} e^{il\phi} \tag{S3}$$

where the beam width $w(z) = w_0\sqrt{1+\frac{z^2}{z_R^2}}$ with w_0 being the beam waist, $R(z) = z + \frac{z_R^2}{z}$ is the radius of curvature, $z_R = \frac{\pi w_0^2}{\lambda}$ is the Rayleigh length, $(2p+|l|+1)\tan^{-1}(\frac{z}{z_R})$ is the Gouy phase and $L_p^{|l|}$ is the associated Laguerre polynomial. The spatial and phase profiles of a $\mathrm{LG}_{l=1,p=0}$ beam is shown in Figure S1. Over the molecular scale, the radial profile $A(r,z)$ is a constant. The OAM beam polarization can be kept linear in the proposed setup and gets absorbed in a Lorentz-polarization factor $|\epsilon_x \cdot \epsilon_s|^2$ in Eq. S1, where ϵ_x and ϵ_s are polarization vectors of the x-ray probe pulse and scattered photon. Using circular polarization just modifies the Lorentz-polarization factor and does not engage with the molecular charge density.

Substituting Eq. S2 in Eq. S1 we obtain for the twisted X-ray diffraction signal

$$S_l(\mathbf{q},T) \propto \int dt\, |E(t-T)|^2 \widetilde{S}_l(\mathbf{q},t) \tag{S4}$$

where $\widetilde{S}_l(\mathbf{q},t) = \langle\hat{\sigma}_l^\dagger(\mathbf{q},t)\hat{\sigma}_l(\mathbf{q},t)\rangle$ is the time-dependent molecular response and $\hat{\sigma}_l(\mathbf{q}) = \int \hat{\sigma}(\mathbf{r})e^{il\phi}e^{i\mathbf{q}\cdot\mathbf{r}}d\mathbf{r}$ is the momentum-space electronic charge-density operator carrying OAM.

Since $\hat{\sigma}^{\dagger}(\mathbf{r}) = \hat{\sigma}(\mathbf{r})$, we have

$$\hat{\sigma}_l^{\dagger}(\mathbf{q}) = \int \hat{\sigma}^{\dagger}(\mathbf{r}) e^{-il\phi} e^{-i\mathbf{q}\cdot\mathbf{r}} d\mathbf{r} = \hat{\sigma}_{-l}(-\mathbf{q}) \tag{S5}$$

Substituting the total time-dependent molecular many-body wavefunction (Eq .1 in main text) in Eq. S4, we obtain

$$\tilde{S}_l(\mathbf{q},t) = \tilde{S}_l^{\mathrm{pop}}(\mathbf{q},t) + \tilde{S}_l^{\mathrm{coh}}(\mathbf{q},t) \tag{S6}$$

where

$$\begin{aligned}\tilde{S}_l^{\mathrm{pop}}(\mathbf{q},t) &= \textstyle\sum_k \rho_{kk}(t) \sum_m \langle \chi_k(t) | \hat{\sigma}_{l,km}^{\dagger}(\mathbf{q}) \hat{\sigma}_{l,mk}(\mathbf{q}) | \chi_k(t) \rangle \\ &= \textstyle\sum_k \rho_{kk}(t) \alpha_{l,kk}(\mathbf{q},t) \end{aligned}\tag{S7}$$

$$\begin{aligned}\tilde{S}_l^{\mathrm{coh}}(\mathbf{q},t) &= 2\Re\left[\textstyle\sum_{j>k} \rho_{jk}(t) \sum_m \langle \chi_k(t) | \hat{\sigma}_{l,km}^{\dagger}(\mathbf{q}) \hat{\sigma}_{l,mj}(\mathbf{q}) | \chi_j(t) \rangle\right] \\ &= 2\Re\left[\textstyle\sum_{j>k} \rho_{jk}(t) \beta_{l,jk}(\mathbf{q},t)\right] \end{aligned}\tag{S8}$$

Because $\alpha_{l,kk}(\mathbf{q},t)$ is real, from Eq. S5 we get $\tilde{S}_{-l}^{\mathrm{pop}}(-\mathbf{q},t) = \sum_k \rho_{kk}(t)\alpha_{-l,kk}(-\mathbf{q},t) = \sum_k \rho_{kk}(t)\alpha_{l,kk}^{*}(\mathbf{q},t) = \tilde{S}_l^{\mathrm{pop}}(\mathbf{q},t)$. This relation does not hold for $\tilde{S}_l^{\mathrm{coh}}(\mathbf{q},t)$ as both $\rho_{jk}(t)$ and $\beta_{l,jk}(\mathbf{q},t)$ are complex numbers.

Note 2. The Purely Electronic Coherence Signal

We now turn to the rotationally-averaged difference signal

$$\Delta S_l(q,t) = \langle \tilde{S}_l(\mathbf{q},t) \rangle_\Omega - \langle \tilde{S}_{-l}(\mathbf{q},t) \rangle_\Omega = \Delta S_l^{\mathrm{pop}}(q,t) + \Delta S_l^{\mathrm{coh}}(q,t) \tag{S9}$$

where q is the magnitude of $\mathbf{q}$ and $\langle \dots \rangle_\Omega$ represents the rotationally-average diffraction signal.

Because $\tilde{S}_l^{\mathrm{pop}}(\mathbf{q},t) = \tilde{S}_{-l}^{\mathrm{pop}}(-\mathbf{q},t)$, we get

$$\Delta S_l^{\mathrm{pop}}(q,t) = \langle \tilde{S}_l^{\mathrm{pop}}(\boldsymbol{q},t) \rangle_\Omega - \langle \tilde{S}_{-l}^{\mathrm{pop}}(\boldsymbol{q},t) \rangle_\Omega = 0 \tag{S10}$$

Eq. S10 demonstrates that the population contribution $\Delta S_l^{\mathrm{pop}}(q,t)$ to signal $\Delta S_l(q,t)$ vanishes.

We thus obtain a purely electronic coherence signal

$$\begin{aligned}\Delta S_l(q,t) = \Delta S_l^{\mathrm{coh}}(q,t) &= \langle \tilde{S}_l^{\mathrm{coh}}(\mathbf{q},t) \rangle_\Omega - \langle \tilde{S}_{-l}^{\mathrm{coh}}(\mathbf{q},t) \rangle_\Omega \\ &= 2\Re\left[\textstyle\sum_{j>k} \rho_{jk}(t) \langle \beta_{l,jk}(\mathbf{q},t) \rangle_\Omega\right] - 2\Re\left[\textstyle\sum_{j>k} \rho_{jk}(t) \langle \beta_{-l,jk}(\mathbf{q},t) \rangle_\Omega\right] \\ &= 2\Re\left[\textstyle\sum_{j>k} \rho_{jk}(t) \langle \beta_{l,jk}(\mathbf{q},t) \rangle_\Omega\right] - 2\Re\left[\textstyle\sum_{j>k} \rho_{jk}(t) \langle \beta_{l,jk}^{*}(-\mathbf{q},t) \rangle_\Omega\right] \\ &= 2\Re\left\{\textstyle\sum_{j>k} \rho_{jk}(t) \left[\beta_{l,jk}(q,t) - \beta_{l,jk}^{*}(q,t)\right]\right\} \\ &= -4 \textstyle\sum_{j>k} \Im\rho_{jk}(t) \Im\beta_{l,jk}(q,t) \end{aligned}\tag{S11}$$

For the thiophenol photodissociation dynamics in this study, the $\Delta S_l(q,t)$ contains contributions from S_2/S_1 and S_1/S_0 electronic coherences with negligible S_2/S_0 electronic coherence. So that

$$\begin{aligned}\Delta S_l(q,t) &= \Delta S_l^{12} + \Delta S_l^{01} \\ &= -4\left(\Im\rho_{12}(t)\Im\beta_{l,12}(q,t) + \Im\rho_{01}(t)\Im\beta_{l,01}(q,t)\right) \end{aligned}\tag{S12}$$

Note 3. Wave Packet Simulations

The quantum dynamical simulations of thiophenol photodissociation involving two CIs have been described in detail previously (*4*). Potential energy surfaces of the S_2, S_1 and S_0 adiabatic electronic states and the nonadiabatic coupling matrix elements of S_2/S_1 and S_1/S_0 were calculated using the SA4-CAS(12,11)/6-311++G(d,p) method, by displacing the molecular structure along the two reactive coordinates (S-H distance and H-S-C angle). Potential energy surfaces and related molecular quantities in two-dimensional space are discretized on a numerical grid with 1024 grid points in S-H distance and 256 grid points in H-S-C angle. The effective Hamiltonian in matrix form comprising three electronic states a (S_0), b (S_1) and c (S_2) is given by

$$\hat{H} = \begin{pmatrix} \hat{T} + \hat{V}_a(\mathbf{R}) & \hat{K}_{ab} & 0 \\ \hat{K}_{ba} & \hat{T} + \hat{V}_b(\mathbf{R}) & \hat{K}_{bc} \\ 0 & \hat{K}_{cb} & \hat{T} + \hat{V}_c(\mathbf{R}) \end{pmatrix} \tag{S13}$$

where $\hat{V}$ are the potential energy surfaces, $\hat{K}_{ab}$ approximates the nonadiabatic couplings between the electronic states a and b. Since there is no conical intersection between S_0 and S_2, the electronic coupling between the electronic states a and c is negligible ($\hat{K}_{ac} = 0$). The kinetic energy operator $\hat{T}$ in Eq. S13 is given in the G-Matrix formalism (*5,6*) according to

$$\hat{T} \simeq -\frac{\hbar^2}{2m}\sum_{o=1}^{2}\sum_{p=1}^{2}\frac{\partial}{\partial q_o}\left[G_{op}\frac{\partial}{\partial q_p}\right] \tag{S14}$$

with $o, p \in \mathbf{R}$ and the G-Matrix computed via its inverse elements

$$(G^{-1})_{op} = \sum_{i=1}^{3N} m_i \frac{\partial x_i}{\partial q_o}\frac{\partial x_i}{\partial q_p} \tag{S15}$$

The nuclear wavepacket is obtained by propagating the S_0 ground state vibrational wavefunction after impulsive excitation to S_2 with a Chebychev scheme (*7*) using 0.05 fs time step. A Butterworth filter (*8*) absorbs the wavepacket at S-H = 10 Å in all three states, as the photodissociation is completed. All terms in the diffraction signals were evaluated every 0.5 fs.

Note 4. Computational Details

The electronic charge densities and transition charge densities in **q**-space (reciprocal space) were evaluated from the state specific charge density matrices, P_{rs}^{jk}, according to

$$\sigma_{jk}(\mathbf{q}, \mathbf{R}) = \int \mathrm{d}\mathbf{r} e^{i\mathbf{q}\cdot\mathbf{r}} \sigma_{jk}(\mathbf{r}, \mathbf{R}) = \int \mathrm{d}\mathbf{r} e^{i\mathbf{q}\cdot\mathbf{r}} \sum_{rs} P_{rs}^{jk}(\mathbf{R}) \phi_r(\mathbf{r}, \mathbf{R}) \phi_s^*(\mathbf{r}, \mathbf{R}) \tag{S16}$$

where $\phi_r(\mathbf{r}, \mathbf{R})$ is an atomic basis function for the r_{th} atomic orbital, j and k are labels for adiabatic electronic states (S_2, S_1 and S_0), **r** and **R** are the electronic and nuclear coordinates. They were evaluated in 0.05 Å increments in the S-H distance and 5° increments in the H-S-C angle. The state specific charge density matrices were calculated by the SA4-CAS(12,11)/6-311++G(d,p) method using the Molpro electronic structure software package (*9,10*). The grid-based $\sigma_{jk}(\mathbf{r}, \mathbf{R})$ in real space was further calculated from the charge density matrices using PySCF software (*11,12*). The twisted x-ray diffraction signals were calculated numerically from Eq. S1 where the profile of LG beams ($p = 0, l = \pm 1$) were used for $\mathcal{A}_l(r, z, \phi)$. The rotational averaging of the diffraction signal was performed numerically, similar to a recent study by Parrish and Martínez (*13*). Since the same algorithm was applied to calculate diffraction signals for $S_{l=1}^{\mathrm{pop/coh}}$ and $S_{l=-1}^{\mathrm{pop/coh}}$, The systematic errors originated from numerical calculations cancel out during the subtraction as is demonstrated in the Figure 2. The subtraction of two independent numerical results $\Delta S_{l=1}^{\mathrm{pop}} = S_{l=1}^{\mathrm{pop}} - S_{l=-1}^{\mathrm{pop}}$ converges to zero, which agrees with the conclusion from our theoretical derivation given by Eq. S10. The q dependence of the numerically calculated $\Delta S_l^{\mathrm{coh}}$ could deviate quantitively from exact analytical results due to the lack of numerical precision. Going further, it will be interesting to extend recently developed analytical methods for calculating isotropic x-ray diffraction signals from ab initio wavefunctions (*14,15,16*) to the twisted x-ray diffraction signals proposed in this study. This could provide quantitively more accurate calculated q-dependent coherence signals given by Eq. S11. We note that in Figure 3 we assumed an impulsive x-ray probe pulse. In practice, an ultrashort x-ray probe pulse with a finite temporal pulse width (< 5 fs) is required to resolve the simulated coherence signal during conical intersection passage.

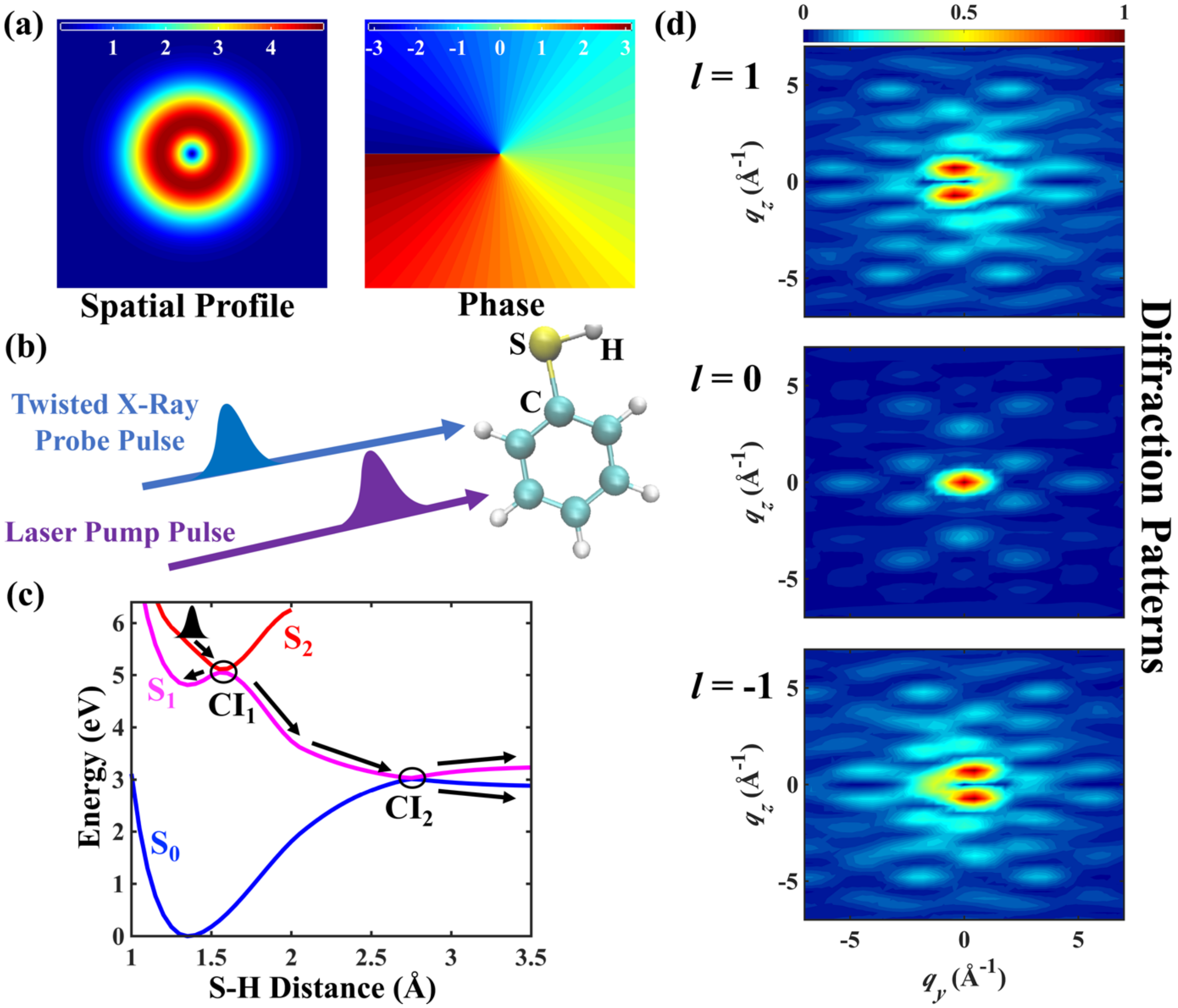

Figure S1. (a) Intensity in arbitrary unit (left) and phase in radians (right) of the $l = 1$ OAM light beam in the transverse plane. (b) The proposed experimental configuration. The photodissociation reaction of thiophenol is initiated by a laser pump pulse, and the resulting time-evolving molecular structure is probed by XRD using twisted x-ray probe pulse with a variable time delay. (c) One-dimensional slice along the S-H distance of our two-dimensional potential energy surfaces for the S_2, S_1 and S_0 adiabatic electronic states of thiophenol calculated at the SA4-CAS(12,11)/6-311++G(d,p) level of theory. Two conical intersections (CI_1: S_2/S_1 and CI_2: S_1/S_0) are marked with open circles. Black arrows sketch the reaction pathway of the nuclear wavepacket initially prepared in S_2. (d) Two-dimensional diffraction patterns of ground-state thiophenol before pump excitation ($S_l^{\mathrm{off}}(\mathbf{q})$) when using x-ray probe pulse with $l = 1$ (top), $l = 0$ (middle) and $l = -1$ (bottom) OAM, respectively. $S_l^{\mathrm{off}}(\mathbf{q})$ are shown in the q_y-q_z plane (q_x=0) for an oriented molecule where its benzene ring is located in the y-z plane.

References

---

1 K. Bennett, M. Kowalewski, J. R. Rouxel, S. Mukamel, Monitoring molecular nonadiabatic dynamics with femtosecond x-ray diffraction. *Proc. Natl. Acad. Sci. U.S.A.* **115**, 6538-6547 (2018).

2 J. R. Rouxel, M. Kowalewski, K. Bennett, S. Mukamel, X-ray sum frequency diffraction for direct imaging of ultrafast electron dynamics. *Phys. Rev. Lett.* **120**, 243902 (2018).

3 L. Allen, M. W. Beijersbergen, R. J. C. Spreeuw, J. P. Woerdman, Orbital angular momentum of light and the transformation of Laguerre-Gaussian laser modes. *Phys. Rev. A* **45**, 8185 (1992).

4 H. Yong, D. Keefer, S. Mukamel, Imaging purely nuclear quantum dynamics in molecules by combined x-ray and electron diffraction. *J. Am. Chem. Soc.* **144**, 7796-7804.

5 P. H. Berens, K. R. Wilson, Molecular dynamics and spectra. I. diatomic rotation and vibration. *J. Chem. Phys.* **74**, 4872–4882 (1981).

6 S. Thallmair, M. K. Roos, R. de Vivie-Riedle, Design of specially adapted reactive coordinates to economically compute potential and kinetic energy operators including geometry relaxation. *J. Chem. Phys.* **144**, 234104 (2016).

7 H. Tal-Ezer, R. Kosloff, An accurate and efficient scheme for propagating the time dependent Schrödinger equation. *J. Chem. Phys.* **81**, 3967–3971 (1984).

8 S. Butterworth, On the theory of filter amplifiers. *Experimental Wireless and the Wireless Engineer* **7**, 536–541 (1930).

9 H.-J. Werner, P. J. Knowles, F. R. Manby, J. A. Black, K. Doll, A. Heßelmann, D. Kats, A. Köhn, T. Korona, D. A. Kreplin, et al., The Molpro Quantum Chemistry Package. *J. Chem. Phys.* **152**, 144107 (2020).

10 H. J. Werner, P. J. Knowles, G. Knizia, F. R. Manby, M. Schütz, Molpro: A General-Purpose Quantum Chemistry Program Package. *Wiley Interdiscip. Rev. Comput. Mol. Sci.* **2**, 242-253 (2012).

11 Q. Sun, T. C. Berkelbach, N. S. Blunt, G. H. Booth, S. Guo, Z. Li, J. Liu, J. McClain, S. Sharma, S. Wouters, et al., PySCF: the Python-Based Simulations of Chemistry Framework. *Wiley Interdiscip. Rev. Comput. Mol. Sci.* **8**, e1340 (2018).

12 Q. Sun, X. Zhang, S. Banerjee, P. Bao, M. Barbry, N. S. Blunt, N. A. Bogdanov, G. H. Booth, J. Chen, Z.-H. Cui, et al., Recent Developments in the PySCF Program Package. *J. Chem. Phys.* **153**, 024109 (2020).

13 R. M. Parrish, T. J. Martínez, Ab initio computation of rotationally-averaged pump-probe x-ray and electron diffraction signals. *J. Chem. Theory Comput.* **15**, 1523-1537 (2019).

14 T. Northey, N. Zotev, A. Kirrander, Ab initio calculation of molecular diffraction. *J. Chem. Theory Comput.* **10**, 4911-4920 (2014).

15 A. Moreno Carrascosa, H. Yong, D. L. Crittenden, P. M. Weber, A. Kirrander, Ab initio calculation of total x-ray scattering from molecules. *J. Chem. Theory Comput.* **15**, 2836-2846 (2019).

16 N. Zotev, A. Moreno Carrascosa, M. Simmermacher, A. Kirrander, Excited electronic states in total isotropic scattering from molecules. *J. Chem. Theory Comput.* **16**, 2594-2605 (2020).